

Dear Author

Please use this PDF proof to check the layout of your article. If you would like any changes to be made to the layout, you can leave instructions in the online proofing interface. First, return to the online proofing interface by clicking "Edit" at the top page, then insert a Comment in the relevant location. Making your changes directly in the online proofing interface is the quickest, easiest way to correct and submit your proof.

Please note that changes made to the article in the online proofing interface will be added to the article before publication, but are not reflected in this PDF proof.

If you would prefer to submit your corrections by annotating the PDF proof, please download and submit an annotatable PDF proof by clicking the link below.

 [Annotate PDF](#)

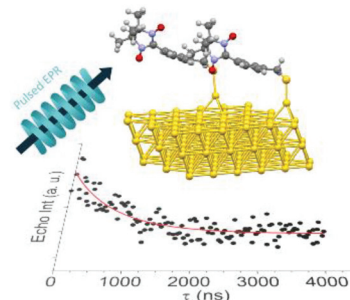
We have presented the graphical abstract image and text for your article below. This briefly summarises your work, and will be presented with your article online.

1

### Chemisorption of nitronyl–nitroxide radicals on gold surface: an assessment of morphology, exchange interaction and decoherence time

Lorenzo Poggini,\* Alessandro Lunghi, Alberto Collauto, Antonio Barbon, Lidia Armelao, Agnese Magnani, Andrea Caneschi, Federico Totti,\* Lorenzo Sorace\* and Matteo Mannini

A multitechnique approach integrated by advanced computational characterization demonstrated the intact chemisorption of nitronyl–nitroxide radicals on Au(111) and allowed determination of its decoherence time.



Please check this proof carefully. Our staff will not read it in detail after you have returned it.

Please send your corrections either as a copy of the proof PDF with electronic notes attached or as a list of corrections. **Do not edit the text within the PDF or send a revised manuscript** as we will not be able to apply your corrections. Corrections at this stage should be minor and not involve extensive changes.

**Proof corrections must be returned as a single set of corrections, approved by all co-authors. No further corrections can be made after you have submitted your proof corrections as we will publish your article online as soon as possible after they are received.**

Please ensure that:

- The spelling and format of all author names and affiliations are checked carefully. You can check how we have identified the authors' first and last names in the researcher information table on the next page. **Names will be indexed and cited as shown on the proof, so these must be correct.**
- Any funding bodies have been acknowledged appropriately and included both in the paper and in the funder information table on the next page.
- All of the editor's queries are answered.
- Any necessary attachments, such as updated images or ESI files, are provided.

Translation errors can occur during conversion to typesetting systems so you need to read the whole proof. In particular please check tables, equations, numerical data, figures and graphics, and references carefully.

Please return your **final** corrections, where possible within **48 hours** of receipt following the instructions in the proof notification email. If you require more time, please notify us by email to [nanoscale@rsc.org](mailto:nanoscale@rsc.org).

## Funding information

Providing accurate funding information will enable us to help you comply with your funders' reporting mandates. Clear acknowledgement of funder support is an important consideration in funding evaluation and can increase your chances of securing funding in the future.

We work closely with Crossref to make your research discoverable through the Funding Data search tool (<http://search.crossref.org/funding>). Funding Data provides a reliable way to track the impact of the work that funders support. Accurate funder information will also help us (i) identify articles that are mandated to be deposited in **PubMed Central (PMC)** and deposit these on your behalf, and (ii) identify articles funded as part of the **CHORUS** initiative and display the Accepted Manuscript on our web site after an embargo period of 12 months.

Further information can be found on our webpage (<http://rsc.li/funding-info>).

## What we do with funding information

We have combined the information you gave us on submission with the information in your acknowledgements. This will help ensure the funding information is as complete as possible and matches funders listed in the Crossref Funder Registry.

If a funding organisation you included in your acknowledgements or on submission of your article is not currently listed in the registry it will not appear in the table on this page. We can only deposit data if funders are already listed in the Crossref Funder Registry, but we will pass all funding information on to Crossref so that additional funders can be included in future.

## Please check your funding information

The table below contains the information we will share with Crossref so that your article can be found *via* the Funding Data search tool. **Please check that the funder names and grant numbers in the table are correct and indicate if any changes are necessary to the Acknowledgements text.**

Funder name	Funder's main country of origin	Funder ID (for RSC use only)	Award/grant number
European Cooperation in Science and Technology	European Union	501100000921	CA15128 MOLSPIN
H2020 Future and Emerging Technologies	Belgium	100010664	Unassigned
Ministero dell'Istruzione, dell'Università e della Ricerca	Italy	501100003407	2015-HYFSRT B96C1700020008
Ente Cassa di Risparmio di Firenze	Italy	501100003056	Unassigned

Q1

## Researcher information

Please check that the researcher information in the table below is correct, including the spelling and formatting of all author names, and that the authors' first, middle and last names have been correctly identified. **Names will be indexed and cited as shown on the proof, so these must be correct.**

If any authors have ORCID or ResearcherID details that are not listed below, please provide these with your proof corrections. Please ensure that the ORCID and ResearcherID details listed below have been assigned to the correct author. Authors should have their own unique ORCID iD and should not use another researcher's, as errors will delay publication.

Please also update your account on our online [manuscript submission system](#) to add your ORCID details, which will then be automatically included in all future submissions. See [here](#) for step-by-step instructions and more information on author identifiers.

First (given) and middle name(s)	Last (family) name(s)	ResearcherID	ORCID iD
Lorenzo	Poggini		0000-0002-1931-5841
Alessandro	Lunghi		0000-0002-1948-4434
Alberto	Collauto		

Antonio	Barbon		0000-0002-2009-5874
Lidia	Armelaio		
Agnese	Magnani	E-7999-2017	0000-0002-6960-9418
Andrea	Caneschi		
Federico	Totti	D-5043-2011	0000-0003-4752-0495
Lorenzo	Sorace		0000-0003-4785-1331
Matteo	Mannini		0000-0001-7549-2124

## Queries for the attention of the authors

Journal: **Nanoscale** Paper: **d1nr00640a**

Title: **Chemisorption of nitronyl–nitroxide radicals on gold surface: an assessment of morphology, exchange interaction and decoherence time**

For your information: You can cite this article before you receive notification of the page numbers by using the following format: (authors), Nanoscale, (year), DOI: 10.1039/d1nr00640a.

Editor's queries are marked like this **Q1**, **Q2**, and for your convenience line numbers are indicated like this 5, 10, 15, ...

Please ensure that all queries are answered when returning your proof corrections so that publication of your article is not delayed.

Query Reference	Query	Remarks
Q1	Funder details have been incorporated in the funder table using information provided in the article text. Please check that the funder information in the table is correct.	
Q2	Please confirm that the spelling and format of all author names is correct. Names will be indexed and cited as shown on the proof, so these must be correct. No late corrections can be made.	
Q3	Text has been provided for footnotes a and b in Table 1, but there do not appear to be corresponding citations in the table. Please indicate suitable locations for the footnote citations.	

# Chemisorption of nitronyl–nitroxide radicals on gold surface: an assessment of morphology, exchange interaction and decoherence time†

Cite this: DOI: 10.1039/d1nr00640a

 Lorenzo Poggini,<sup>1</sup> Alessandro Lunghi,<sup>2</sup> Alberto Collauto,<sup>3</sup> Antonio Barbon,<sup>4</sup> Lidia Armelao,<sup>5</sup> Agnese Magnani,<sup>6</sup> Andrea Caneschi,<sup>7</sup> Federico Totti,<sup>8</sup> Lorenzo Sorace<sup>9</sup> and Matteo Mannini<sup>10</sup>

A combined ToF-SIMS, XPS and STM characterization has been adopted here to study the deposition of a sulphur-functionalized nitronyl nitroxide radical on Au(111) clearly demonstrating the chemisorption of intact molecules. EPR characterization showed that the radical molecules maintain their paramagnetic character. Pulsed EPR measurements allowed to determine the decoherence time of the nanostructure at 80 K, which turned out to be comparable to the one measured in frozen solution and longer than previously reported for many radicals and other paramagnetic molecules at much lower temperatures. Furthermore, a state-of-the-art *ab initio* molecular dynamics study has been performed, suggesting different possible scenarios for chemisorption geometries predicting the energetically favoured geometry. The calculated magnetic properties indicate a partial non-innocent role of the gold surface in determining the magnetic interactions between radicals in packed structures. This suggests that the observed EPR spectrum is to be attributed to low-density domains of disordered radicals interacting *via* dipolar interactions.

 Received 29th January 2021,  
Accepted 24th March 2021

DOI: 10.1039/d1nr00640a

rsc.li/nanoscale

## Introduction

Monolayers of magnetic molecules are attracting broad interest thanks to their potential technological applications as building block units in new devices for molecular spintronics<sup>1</sup> and

quantum computation.<sup>2,3</sup> A crucial step in this direction is the control of the deposition of magnetic material forming a single layer. Self-assembling of monolayer (SAM)<sup>4</sup> is one of the most used techniques to achieve a bidimensional array of (quasi-)ordered molecules absorbed on the surface from diluted solution. Prerequisite of the SAMs formation is the introduction of functional groups allowing specific (covalent) interactions with a given surface. A 2D regular structure can then be obtained by optimizing intermolecular interactions between nearest neighbours.<sup>4</sup> This strategy can be extended to molecules featuring specific functionalities, such as magnetic or optical properties. In the case of polynuclear clusters behaving as Single-Molecule Magnets (SMM),<sup>5</sup> previous studies showed that this fine control is only partially achievable due to their steric hindrance and to their multiple grafting arrangements,<sup>6–8</sup> while it has been successfully employed for organic radicals.<sup>9–16</sup> During the last decade different approaches were used to deposit pure organic radical molecules on surfaces using either High Vacuum (HV)/Ultra High Vacuum (UHV)<sup>16–22</sup> approaches or wet chemistry (*i.e.* Langmuir–Blodgett and SAM).<sup>9,13,23</sup> However, to date, only a few of papers have tackled the adsorption of the pure organic radicals at the computational level.<sup>24</sup>

The interest toward nitronyl–nitroxide radicals (Nit) germinated from the observation of long-range magnetic order at

<sup>1</sup>Department of Chemistry “Ugo Schiff” and INSTM Research Unit, University of Florence, I-50019 Sesto Fiorentino, Italy. E-mail: lorenzo.sorace@unifi.it

<sup>2</sup>ICCOM-CNR, via Madonna del Piano 10, 50019 Sesto, Fiorentino, Italy.

E-mail: lpoggini@iccom.cnr.it

<sup>3</sup>Department of Chemical Sciences and INSTM Research Unit, University of Padua, I-35131 Padova, Italy

<sup>4</sup>Institute of Condensed Matter Chemistry and Technologies for Energy, National Research Council of Italy, ICMATE-CNR, via Marzolo 1, 35131 Padua, Italy

<sup>5</sup>Department of Chemical Sciences and Materials Technologies, National Research Council of Italy, DSCTM - CNR, Piazzale A. Moro 7, 00185 Rome, Italy

<sup>6</sup>Department of Biotechnologies, Chemistry and Pharmacy, and INSTM Research Unit, University of Siena, I-53100 Siena, Italy

<sup>7</sup>DIEF - Department of Industrial Engineering and INSTM Research Unit, University of Florence, Via S. Marta 3, I-50139 Florence, Italy

† Electronic supplementary information (ESI) available: Experimental section; computational details; additional XPS data and analysis; ToF-SIMS data and analysis; STM images; additional EPR data and computation results, as figures and tables. See DOI: 10.1039/d1nr00640a

‡ Present address: School of Physics, CRANN Institute, AMBER centre, Trinity College, Dublin 2, Ireland.

§ Present address: Goethe-Universität Frankfurt am Main.

low temperature in bulk phases<sup>25</sup> and from the possibility of using them as building blocks of more complex magnetic structures such as Single-Chain Magnets.<sup>26–28</sup> Nowadays the key interest for potential magneto-transport and quantum computation purposes is related to the spin dynamic properties of **Nits**: they feature relatively long spin–lattice ( $T_1$ ) and significant decoherence ( $T_2$  or  $T_m$ ) times in frozen solutions at a temperature as high as liquid nitrogen and without the need of using deuterated or proton-free solvents.<sup>29</sup> Thanks to these properties and their inherent quantum nature, they have also been proposed, together with other radical families, as potential molecular-based qubits, or as elements of spintronics devices.<sup>30–36</sup> Indeed, recent works suggest that **Nit** function can be used to influence the spin injecting electrode in hybrid vertical spin valves.<sup>34</sup> In this perspective, the investigation of the decoherence properties of organic radicals organized in addressable arrays on surfaces is a key point in the quest for technological use of these systems. However, to the best of our knowledge, this issue has not been addressed yet. We aim to move a step forward in this direction by reporting here a complete characterization of a SAM of a sulphur-functionalized **Nit**, the thioacetic acid 4-(nitronyl–nitroxide radical) benzyl ester (**1**, Fig. 1a), on Au(111) including a first attempt of evaluating the spin relaxation properties of this monolayer. A complete description of the system is obtained by combining time-of-flight secondary ion mass spectrometry (ToF-SIMS) and X-ray Photoelectron Spectroscopy (XPS) to provide the chemical characterization of the chemisorbed monolayer and room temperature scanning tunnelling microscopy (STM) to achieve a morphological characterization of the deposit. The characterization of the static and dynamic magnetic properties of the nanostructured radical has been achieved by continuous-wave (cw) and pulsed electron paramagnetic resonance (EPR) spectroscopy. This set of experiments has been flanked by a state-of-art theoretical investigation as *ab initio* molecular dynamics (AIMD) to get further insights about the favoured chemisorption configuration and static DFT approach for the calculations of intermolecular magnetic interactions in the SAM.

## Results

### SAM preparation and chemical characterization

The synthetic strategy adopted to introduce the thioacetic group needed to promote the chemisorption of the **Nit** moiety on gold has been described elsewhere.<sup>37</sup> Here we focused on the characterization of the SAMs of **1**, which were prepared by incubating a hydrogen-flame annealed slab of gold<sup>9,38</sup> in a 3 mM solution of **1** in dichloromethane under reflux condition for 24 hours in the dark.<sup>9</sup> After the incubation procedure the spontaneous and quantitative (75%) removal of the thioacetyl protection and the formation of a chemical bond between the sulphur of the linker group and the gold surface has been confirmed by using in-house XPS analysis (see Fig. 1 and Table S1†). The XPS spectra of the SAM sample show the presence of clearly detectable intense peak in the S 2p<sub>3/2</sub> region at 161.8 eV, a binding energy (BE) that is lower than the one found in the bulk sample obtained by drop-cast (163.7 eV) (see Fig. 1b). The ratio and BE difference between components S 2p<sub>3/2</sub> and S 2p<sub>1/2</sub> is maintained in passing from the bulk (drop cast) to the chemisorbed sample. The further presence of spectral features at 163.7 eV and 168.4 eV points to a small number of physisorbed molecules (less than 16%) and minimal oxidation of the linking group (14%) that significantly support the compactness of the obtained monolayer.<sup>39,40</sup> As for the N 1s region, XPS spectra of both the bulk phase and the SAM evidence the onset of an X-ray induced photoreduction process occurring at the nitrogen. Indeed, in addition to the principal component at 403.6 eV (Fig. 1c) which is typical for **Nit** systems,<sup>18</sup> another component at 399.7 eV is observed in the bulk of **1**, the intensity of which increases on increasing X-ray exposure (see Fig. S1†). The peak has been attributed to nitrogen atoms in N–H group forming upon photoreduction. Beside this, we point out the presence of a weak additional contribution at 397.5 eV, which supports the presence of a small fraction of molecules (*ca.* 8%) in which nitrogen atoms are involved in a direct Au–N bond.<sup>17</sup> Within the error limits, the semi-quantitative analysis obtained by integrating the

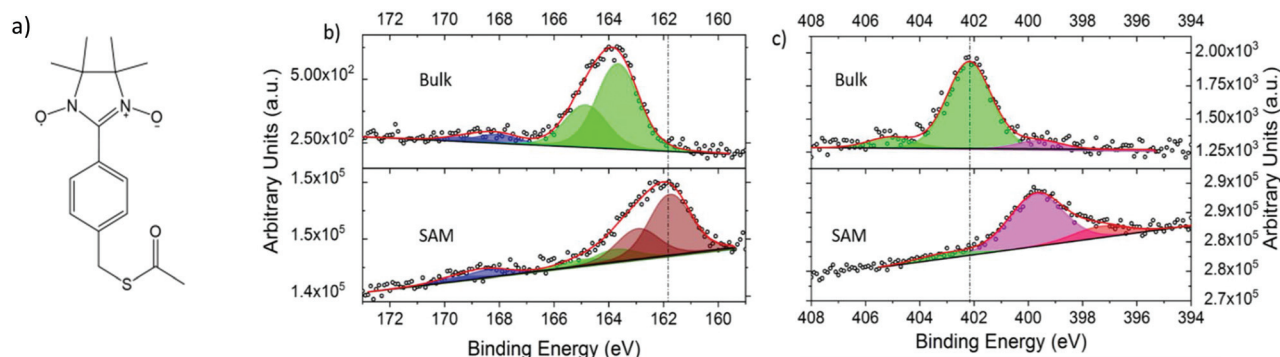


**Fig. 1** (a) Chemical structure of thio-acetic acid 4-(nitronyl–nitroxide radical)benzyl ester, **1**; XPS spectra of **1** in the S 2p region (b) and in the N 1s region (c) in bulk (drop cast) and on surface evidencing the contributions from the different spectral components required for least squares fitting. In (b) green curves correspond to R–S–Ac component, while brown ones to R–S–Au component of the S 2p signal. In (c) green curves correspond to R–NO N 1s component while pink ones to R–N–H N 1s component.

whole S 2p and the N 1s XPS signals, reveals a good agreement of the N/S ratio with the theoretical expectations (2.0) both for the bulk sample obtained by drop-casting on gold (1.9) and for the SAM (1.6) (see Table S1 and XPS experimental details in ESI†). This result supports the hypothesis that chemisorption does not alter the molecular framework.

ToF-SIMS<sup>41</sup> characterization of the SAM further confirms the occurrence of chemisorption of the intact system, showing some relevant signals not detected in the bulk material at 505.3 *m/z*, 461.3 *m/z*, 447.3 *m/z* and 445.3 *m/z*: according to our analysis (see Fig. S2 in ESI and Table S2†) these can be attributed to a gold atom directly interacting with the sulphur atom of the molecular backbone. In particular, the isotopic pattern centred at 461.3 *m/z* (Fig. S2d†) can be correlated to a  $[M-O-Ac + 2H + Au]^+$  fragment, observable only in SAM sample due to the chemical grafting with Au. The assignments for the lower *m/z* peaks (247.1–323.1 *m/z*) reported in Table S2† both for SAM and the bulk, are obtained by considering the simultaneous loss of oxygen atoms from the nitroxide function followed by the typical rearrangement observed in other Nit bulk system.<sup>9</sup> The formation of a single layer deposit is further corroborated by the room temperature STM characterization we reported in Fig. S3:† indeed, this experiment in air, reveals the presence of the typical defects of SAMs (pinholes)<sup>42</sup> thus excluding the formation of multi-layered structure. Thanks to those characterization we can assume that the chemical structure and the stoichiometry are retained after the wet chemistry deposition process.

### EPR spectroscopy

EPR spectroscopy (see ESI† for Experimental details) has been used as a key tool for the characterization of the magnetic properties of the monolayer of **1**. The room-temperature cw-EPR spectrum (Fig. 2) of the SAM of **1** is similar to the one reported for other nitronyl–nitroxide derivatives assembled on gold,<sup>9,11</sup> with clear evidence of the hyperfine pattern due to the coupling of the unpaired electron with the two equivalent <sup>14</sup>N (*I* = 1) nuclei. The observation of a spectrum with resolved hyperfine features close to those of **1** in toluene solution testifies that the paramagnetic character is preserved after chemisorption and further confirms that the process occurs by maintaining the integrity of the Nit function (*i.e.* without degradation to the corresponding imino-nitroxide). A qualitative analysis of the cw-EPR spectra of the SAM of **1** at different temperatures (Fig. 2a) evidences a narrowing of the homogeneous linewidth on increasing temperature. The relatively narrow, powder-like, lines observed at room temperature, indicate that the dynamics in this temperature range fall into a fast motion regime with restricted width. This hypothesis is also in line with the relatively easy saturation, which can be observed already at 20 dB (Fig. S4†). In agreement with such a fast dynamics and the consequent absence of any long-range geometric order, no angular dependence of the EPR spectrum has been observed at room temperature (Fig. S5†). Moreover, the observed spectral pattern at 294 K is rather similar to the one observed in frozen toluene solution at 80 K, but with a

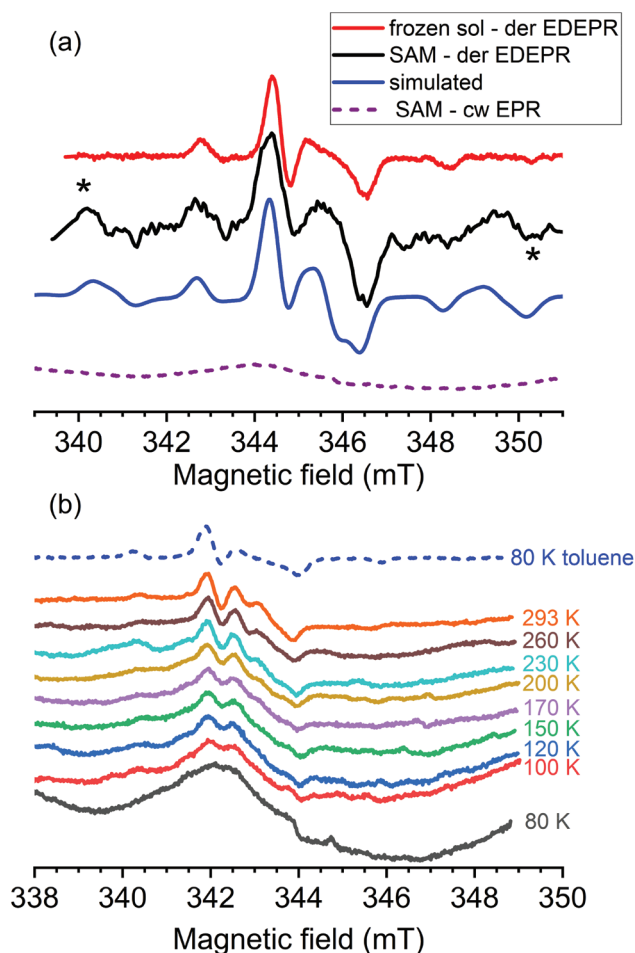


**Fig. 2** (a) Temperature dependence of the X-band cw-EPR spectrum of a SAM of **1**. The cw-EPR of **1** in toluene (ToI) at 80 K is reported for reference. (b) Comparison of the derivative Echo detected spectra at 80 K and  $\tau = 200$  ns for SAM sample (black) and for the toluene solution (red). The asterisks highlight the extra bands present in the SAM sample. In blue the simulation of the SAM sample (reported in Table S3†) by using parameters close to those obtained for the thio-acetic acid 4-(nitronyl-nitroxide radical)benzyl ester in toluene frozen solution.<sup>31</sup> The simulation of the side bands is relative to a pair of radicals with a dipolar interaction of  $|D| = 510$  MHz with the largest direction of interaction approximately along the Z-component of the <sup>14</sup>N tensor, by supposing that they stack face-to-face. For comparison, the cw-EPR of the SAM sample at the same temperature is given (dashed line).

reduction of the total width by *ca.* 0.5 mT. This observation is the main evidence of a restricted mobility, faster at higher temperatures, which leads to a partial averaging of the z-component of the hyperfine interaction. From the reduction of the spectral width, we estimate an amplitude of *ca.* 17°. Because of internal constraints, the major contribution of the motion is likely a twist around the phenyl C1–C4 axis, but a twist around the carbon–sulphur  $\sigma$ -bond can also contribute (see further). These rotational/librational degrees of freedom of radicals are consistent, at high temperature, with a full isotropization of the EPR spectrum, and support the hypothesis of a low-density packing of **1** on the Au surface. Furthermore, the large line



broadening, well visible at 80 K, indicates a slowdown of the motion and the onset of splitting from electron–electron interactions (see below).

In order to study both the dynamics and the spin–spin interaction, we attempted to record echo–detected EPR (EDEPR) spectra for the SAM of **1** close to liquid nitrogen temperature. Despite the small amount of sample ( $<10^{14}$  spins) we were able to observe a definite spectrum after 12 h acquisition (Fig. 3a and c). This is the first important indication that the decoherence time for a consistent part of the sample is long, and therefore, the detection of a measurable echo was possible.

The lineshape of the derivative of the echo-detected spectrum of the SAM of **1** at 80 K is rather similar to that of **1** obtained in frozen toluene (Fig. 2b),<sup>29</sup> but different with respect to the cw-EPR spectrum of **1** in the SAM at low temperature. These observations point to the formation of SAM domains of **1** with different mobility of the radical and/or different spin–spin interaction. Radicals with low mobility and small spin–spin interactions result in domains where the molecules are isolated, having a residual librational motion larger than in toluene, and which accounts for the slightly larger linewidth.

In the EDEPR spectrum (Fig. 2b), we note the clear presence of narrow sidebands, indicating a definite spin–spin interaction. These bands could be reproduced in the simulation<sup>44</sup> by assuming that the spectrum is a superposition of different contributions: isolated (the majority) and mildly interacting spins (dipolar interaction). The best reproduction of the spectra was obtained by assuming  $|D| = 510$  MHz, (corresponding to a distance of *ca.* 5.3 Å) along the nitrogen  $p_z$ -axes (see Table S3† for best simulation parameters).

To determine the decoherence time  $T_m$  of these samples, Hahn echo decay curves (Fig. 3b and d) were measured at 80 K and 120 K (Fig. 3c and d) by removal of the off-resonance

decay signal from the on-resonance one. These curves were fitted to the expression:

$$I(2\tau) = I_0 + A_f \exp(-2\tau/T_{m,f}) + A_s \exp(-2\tau/T_{m,s}) \quad (1)$$

where  $\tau$  is the inter-pulse delay time,  $A_f$  and  $A_m$  account for the relative contributions of the fast and slow components and  $T_{m,f}$ ,  $T_{m,s}$  are the corresponding decay times. The first component, with low weight, is attributed to a non-perfect subtraction of the off-resonance signal, while the second one is the actual relaxation of the radical SAM. At 80 K, the best fit parameters were  $T_{m,f} = 0.2 \pm 0.2$   $\mu$ s and  $T_{m,s} = 5 \pm 1$   $\mu$ s with a relative weight of  $A_f = 1.0$  and  $A_s = 0.3$ . At 120 K the fast component (background) signal is strongly reduced and the lineshape of the EDEPR is slightly different. Fit of the Hahn decay gave a phase memory time of  $T_m = 1.5 \pm 0.2$   $\mu$ s.

On the other hand, cw-EPR spectra at low temperature shows, superimposed to the signals of the domains determined by spin-echo methods, a broad and almost featureless band. In order not to be detected by EDEPR the relaxation times of the species responsible for this signal must be fast. Two possible reasons can be invoked for a shortening of the relaxation times: a slow-motion regime that induce a broadening of the lines or the onset of exchange interactions.

### Computational results

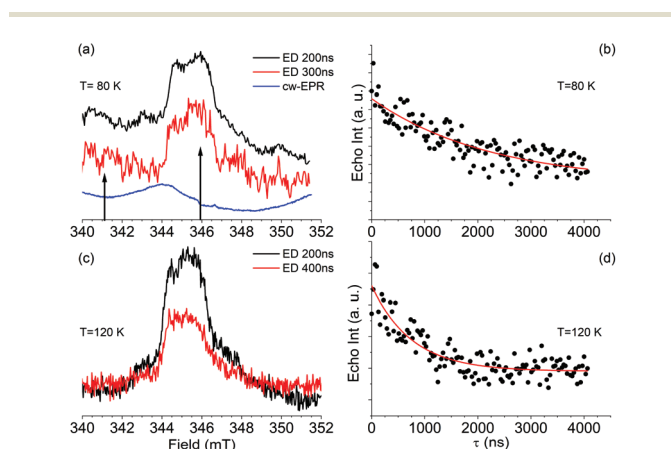
A computational study was undertaken to get a more detailed comprehension of the structure and morphology of the radical chemisorbed on surfaces, as well as to pave the way for further theoretical and experimental investigations focused on the dynamic properties of this system. The chosen approach is based on the ones reported elsewhere.<sup>6–8,45,46</sup> Two different model substrates were considered, namely an unreconstructed (**Au<sub>clean</sub>**) and reconstructed (**Au<sub>recon</sub>**, see ESI† for computational details) gold surfaces. For both surfaces, calculations point to a high symmetry arrangement of the radicals, the two differing in the binding modes for the sulphur atoms: in a bridge position for radicals on **Au<sub>clean</sub>** (**1@Au<sub>clean</sub>** hereafter) and atop the adatoms for radicals on **Au<sub>recon</sub>** (**1@Au<sub>recon</sub>** hereafter), see Table 1.

Both scenarios resulted in a regular and almost identical hexagonal pattern, with the radicals laying orthogonal to the surface.

This suggests that any reconstruction of the surface would not significantly affect the symmetry and the geometrical parameters of the unit cell of the adsorbed radicals.

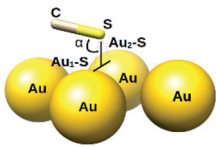
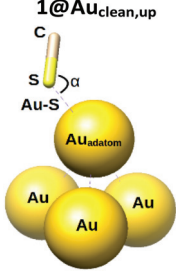

To check for this point, the time evolution of the functionalized surface was calculated by AIMD for both cases. In the **1@Au<sub>clean</sub>** scenario, all the radicals start relaxing from their stand-up positions (**1@Au<sub>clean,up</sub>** from now on) to a laid-down conformation (**1@Au<sub>clean,down</sub>** from now on), which is maintained to the end of the thermalization stage and for all the following simulation time (see Fig. S6†).

Interestingly, each radical adheres to the surface along the same direction, leading to an almost regular pattern of their NO groups. This conformation (**1@Au<sub>clean,down</sub>**) gives an enthalpic gain of 27.7 kcal mol<sup>-1</sup> with respect to the starting



**Fig. 3** Echo detected EPR spectra (left) of a SAM of **1**, acquired with different delay times at 80 K (a) and 120 K (c). Corresponding Hahn echo decays as obtained from on-resonance conditions minus off-resonance conditions (see arrows) at the same temperatures are reported in panel (b) and (d).

**Table 1** Calculated geometrical parameters of **1** adsorption after optimization: the schematic representation of the Nit molecule is limited to the carbon and sulphur atoms for clarity sake

Cell	Position	Au <sub>1,2</sub> -S, Å	Au <sub>1,2</sub> -S-C α, °
	Bridge	2.55(3) 2.71(7)	101.8(2) 121(5)
	Atop	2.33(1)	106.4(2)
	<b>1@Au<sub>recon,up</sub></b>		

<sup>a</sup> Values in parenthesis are presented to show the differences within two geometrical “equivalent” adsorption pairs in Au<sub>clean</sub>. <sup>b</sup> Values in parenthesis are presented to show the differences within two geometrical “equivalent” adsorption pairs Au<sub>recon</sub>.

one and suggests that at this level of coverage dispersive forces and  $\pi$ - $\pi$  interactions are not efficient enough to make an upstanding conformation likely.

For **1@Au<sub>clean,down</sub>**, the AIMD run evidences a distribution of the gold surface–nitroxide (Au–(N)O) distances in the range of  $\sim 1$  Å to  $\sim 7$  Å, with two maximal probability values of 2.2 and 4.2 Å (see ESI Fig. S7†). At these distances the  $\pi^*$  orbital of NOs groups is expected to directly overlap with the gold surface electron density, with a consequent possible transfer of the unpaired electron to the reservoir of gold electronic bands. The two inequivalent NOs groups are lying between  $\sim 3$  Å and  $\sim 7$  Å from the gold surface, which is consistent with what has been found in similar system.<sup>9,46</sup> Denser coverages have been tested but they led to decomposition of at least one Nit. These results suggest that the steric hindrance of nitronyl–nitroxide groups cannot be compensated by attractive dispersion forces. This is further confirmed by the distribution of the binding sulphur atoms with respect to the gold atoms of the first layer (Fig. 4) and by the analysis of sulphur atoms coordination numbers spanned throughout the AIMD (Fig. S8†). The results reported in Fig. 4 further indicate that the sulphur atoms mobility is quite low with no evidence of diffusion. Indeed, the grafting S sites are localized with a range of S–S distances of 8.3–9.3 Å.

As for the **1@Au<sub>recon</sub>** scenario, the AIMD runs show a prompt change of the local geometry of the Au–S. Indeed, the sulphur atoms move from atop the gold adatom to a staple position (see Fig. S9†). Immediately after, as already observed for the **1@Au<sub>clean</sub>** case, a relaxation of the radicals from an upstanding conformation to a laid down one was calculated. A

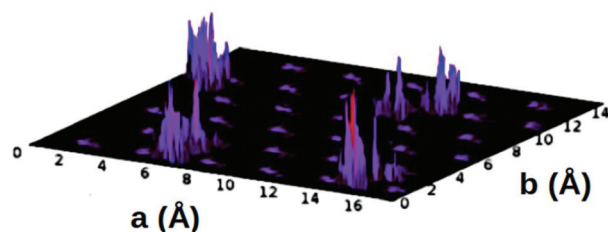


**Fig. 4** Probability of finding sulphur atoms on the gold surface. Darker colours are associated to low probability (lower peaks) while brighter ones to high probability (higher peaks). Small smooth spots in the hexagonal pattern represent the possible positions of the gold atoms of the first layer for which the probability has been removed for sake of clarity. The dimensions of a and b are the ones of the simulation cell (see ESI†).

large enthalpic gain of 30.02 kcal mol<sup>-1</sup> was observed also in this case. At variance with **1@Au<sub>clean</sub>**, the NOs groups did not arrange in an ordered pattern and gave a larger number of different quasi-degenerate conformations. However, it is likely that a higher order might be eventually reached by increasing the time used to study the conformational space. Interestingly, in this new structure (**1@Au<sub>recon,down</sub>** hereafter), we observe an oxygen atom of a NO group directly interacting with an adatom (O–Au<sub>adatom</sub> = 2.41 Å, see Fig. S9b†).

Therefore, AIMD indicates that **1@Au<sub>clean,down</sub>** and **1@Au<sub>recon,down</sub>** represent the most likely scenarios mimicking experimental highly packed SAMs if the thermodynamic data are considered. This is in contrast with previous reports on other Nit<sup>45,46</sup> and different organic radical based SAM,<sup>47</sup> where the temperature effects are not taken into considerations. In this regard, these results are of great importance since indicate the necessity to take them into consideration to properly describe the grafting process when a system with a great structural mobility is considered.

Theoretical investigations may also provide useful information for the analysis of the magnetic properties of the SAM. As a first step, we calculated the spin density for different optimized structures obtained from different anchoring scenarios of a single Nit radical suggested by AIMD as guess geometries (Fig. S9†). Unreconstructed gold surface was considered as reference (Table 2, see ESI† for details). It is worth to stress

**Table 2** Computed spin density values (a.u.) for a single Nit radical with different bonding configurations for a gold clean surface: standing configuration (**1@Au<sub>clean,up</sub>**), and lying down configuration, with single Nit oriented either parallel **1@Au<sub>clean,down,||</sub>** or orthogonal to the surface **1@Au<sub>clean,down,L</sub>**. **1<sub>isol</sub>** is the radical in vacuum

Atom	<b>1<sub>isol</sub></b>	<b>1@Au<sub>clean,up</sub></b>	<b>1@Au<sub>clean,down,L</sub></b>	<b>1@Au<sub>clean,down,  </sub></b>
O1	0.33	0.28	0.25	0.26
O2	0.33	0.28	0.32	0.27
N1	0.26	0.22	0.23	0.21
N2	0.26	0.22	0.22	0.21
C <sub>α</sub> <sup>a</sup>	-0.16	-0.13	-0.15	-0.13
Total	1.03	0.88	0.87	0.82

<sup>a</sup>  $\alpha$ -Carbon atom of the nitronyl–nitroxide group.

**Table 3** Computed exchange couplings ( $\text{cm}^{-1}$ ) and ground states for the four possible configurations of radicals on gold surfaces and the two scenarios where gold surface has been removed ( $\mathbf{1Au}_{\text{clean,up}}$  and  $\mathbf{1Au}_{\text{clean,down}}$ ) computed with PBE functional. In parenthesis, the values computed with B3LYP functional (see ESI† for more details)

	$J_1$	$J_2$	$J_3$	$J_4$	GS
$\mathbf{1Au}_{\text{clean,up}}$	-0.08 (-0.21)	-0.04 (0.07)	-0.08 (-0.10)	-0.05 (0.03)	
$\mathbf{1Au}_{\text{clean,down}}$	-0.18 (-0.39)	0.26 (0.19)	0.14 (0.07)	0.29 (0.08)	
$\mathbf{1@Au}_{\text{clean,up}}$	-0.06	-0.03	-0.08	-0.05	$S = 2$
$\mathbf{1@Au}_{\text{clean,down}}$	3.22	-6.93	-0.38	7.41	$S = 1$
$\mathbf{1@Au}_{\text{recon,up}}$	-0.05	-0.04	-0.09	-0.03	$S = 2$
$\mathbf{1@Au}_{\text{recon,down}}$	6.24	-6.57	-1.60	5.12	$S = 0$

that the single molecule optimizations can be also considered as mimicking the low-density scenario *vs.* the closed packed one represented by the AIMD unit cells. Overall, a reduction of the spin density for both N and O (<25%) with respect to that of the isolated molecules is observed for all scenarios. This result indicates that the gold surface plays a role in the modulation of the magnetic properties of the single Nit. However, the presence of a direct overlap of the  $\pi^*$  orbitals with the gold conductive bands does not significantly quench the paramagnetic character of the Nit radical. This is particularly evident for lying down radical configuration, with single Nit oriented orthogonal to the surface ( $\mathbf{1@Au}_{\text{clean,down,L}}$ ), showing a larger quenching (0.07 a.u.) for the oxygen atom closest to the surface (O1), while for the non-interacting one (O2) a decrease of only 0.01 a.u. is observed. These results are of much relevance since they support the EPR evidence of the persistence of the radical species upon adsorption and prompted us to simulate the STM images for the four conformations at 0.65 V (empty states).

In all the four scenarios, a hexagonal unit cell  $A \times B$  was computed, with features which qualitatively agree with the experimental ones (see ESI, text, Fig. S10 and Table S4†), thus not allowing to draw definite conclusions.

With the aim of obtaining clearer indications on the preferred configurations, we theoretically investigated the possibility of exchange coupling magnetic interactions among the Nit radicals. Different exchange couplings were computed for the four possible conformations, leading to different ground states (see Table 3). The calculated magnetic interactions among the nitroxide centres in both  $\mathbf{1@Au}_{\text{clean,up}}$  and  $\mathbf{1@Au}_{\text{recon,up}}$  scenarios are very small, of the orders of few  $10^{-2} \text{ cm}^{-1}$  (comparable with the SCF convergence criterium). On the other hand,  $\mathbf{1@Au}_{\text{clean,down}}$  and  $\mathbf{1@Au}_{\text{recon,down}}$  scenarios show much larger magnetic interactions of the order of  $1\text{--}2 \text{ cm}^{-1}$ . This indicates that the surface plays a role in the propagation of the magnetic information among the radical centres and it is thus non-innocent. This is supported by the independence of  $J$ 's from the radical-radical distance, which indicates that direct overlap among the NO groups cannot be considered responsible for the calculated interactions. Spin densities plots for all the scenarios show a delocalization in the gold surface supporting its non-innocent role as super-exchange bus (Fig. S11†). Further proves of its active role is witnessed by the results obtained for model systems where the

gold surface is removed (identified as  $\mathbf{1Au}_{\text{clean,down}}$  and  $\mathbf{1Au}_{\text{clean,up}}$  hereafter). In the case of the lying down conformation, the magnitude of the exchange interactions drops of almost two orders of magnitude when the gold surface is not included (see Table 3). It is worth to mention that the computed  $J$  for laid down configurations, where a super-exchange pathway *via* gold surface is established, are somehow biased by in their magnitude by the use of pure DFT (antiferromagnetic contributions over-estimated). It is also evident that the inclusion of the dispersion forces corrections was determinant in getting more reliable geometries with respect to the ones found in ref. 45. Indeed, the computed  $J$  for the standing up scenarios are found similar in magnitude to the ones found in crystals for similar compound.<sup>48</sup>

## Discussion

The experimental characterization of the SAM of **1** showed unequivocally that it is safely chemisorbed on gold surface. The EPR results and the theoretical calculations allow to conclude that formation of the SAM occurs maintaining the paramagnetic character of the molecule and that the deposited molecules are characterized by fast dynamics (in the EPR time-scale) and a restricted motion within cones of about  $20^\circ$ . Indeed, at high temperature, we observe an EPR spectrum which is quite close to that of the frozen solution. The spectrum is attributed to radicals with restricted mobility in fast motion regime, and, because of the relatively large adsorption enthalpy (of the order of  $30 \text{ kcal mol}^{-1}$ ), likely the motion is a twist of the Nit group along its axis over the surface. Such motion can explain the reduction of the  $^{14}\text{N } A_{zz}$  components.

From the thermodynamic point of view the most favourable calculated scenarios are those for which the radicals lay down on the surfaces, driven by the interaction of the phenyl and NO groups with the gold surface. DFT calculations also point to a non-innocent role of the surface, which transmits a relevant intermolecular exchange interaction between radicals, dependent on the absorption configuration. This is consistent with the observation of the Kondo effect in the weak coupling regime<sup>49</sup> for a different nitronyl-nitroxide radical on Au(111) where the magnetic impurities could be injected directly by the Nit itself through the homolytic break of the  $\text{--S--Ac}$  in the conduction bands as already suggested previously.<sup>45,46,50,51</sup>

1 Therefore, a magnetic interaction between impurities  
leading to magnetic ordering may arise<sup>52</sup> if the spin cor-  
relation generated by the radical-conduction electrons is pre-  
served by the electrons which then interact with the other  
5 radical. This interaction is therefore expected to be strongly  
dependent on the temperature, if thermal relaxation processes  
can interfere in the transfer of the spin correlation. Therefore,  
the DFT magnetic calculations accounts for a low-temperature  
10  $J$  value.

10 The interaction with the surface, while of fundamental  
importance to transmit the exchange interaction, does not  
appear however to be large enough to quench the paramag-  
netic properties of the radical contrarily to what reported pre-  
viously by different authors<sup>53,54</sup> On the other hand, the  
15 strength of exchange coupling, while depending on the  
absorption configuration, is always calculated to be much  
larger than the hyperfine coupling to the nitrogen nuclei.  
Thus, for a compact monolayer of radicals an EPR spectrum  
much different from that of an isolated one would be expected.  
20 A single exchange-narrowed, dipolar broadened line has been  
indeed reported by different groups.<sup>47,55,56</sup> For those systems,  
however, the standing conformation was suggested to be the  
favoured one due to the structural features of the radicals. No  
25 temperature effects were taken into consideration though.  
Consequently, the exchange interaction was of the direct type  
and not mediated by the surface.

In the case of the SAM of **1**, exchange interactions are not  
visible at room temperature because of the relatively large  
30 mobility, able to average direct interaction, and because of the  
temperature, which quenches the interaction with the surface.

The disorder in the orientation of Nit radicals is further  
supported by the absence of measurable angular dependence.

35 At lower temperature EPR spectra evidence the presence of  
different domains. One is made up by slow relaxing radicals,  
observed by EDEPR; this suggests that they are located in  
environments that disfavour exchange interactions, *i.e.* in low-  
density packing regions. For some of these the dipolar pair-  
wise interaction is visible. The second domain is evidenced by  
40 the broad featureless band in CW EPR, which are attributed to  
the tightly packed regions with non-negligible exchange inter-  
actions, as suggested by calculations.

45 The combination of calculations and spectroscopy then  
allows us to draw a very precise picture of the structure and  
properties of the sample. This is of particular interest since  
the isolated radicals maintain their long decoherence time, as  
observed by pulsed EPR. At 80 K the measured  $T_m$  is indeed  
comparable to the one measured in frozen solution<sup>29</sup> and  
50 longer than previously reported for many radicals and other  
paramagnetic molecules at much lower temperatures<sup>57</sup> and of  
the same order of magnitude of the Blatter radical in frozen  
solution.<sup>20</sup> While this is an important step toward the use of  
55 these systems in potential spintronics or QC devices, its attri-  
bution to disordered, low density packed radicals, suggests  
that future efforts must be aimed at obtaining an improved 2D  
order of the deposited radical, possibly on more innocent  
surfaces.

## Summary and conclusions

1 Tof-SIMS, XPS and STM demonstrated that the thioacetic 4-  
(nitronyl-nitroxide radical)benzyl ester on Au(111) forms a  
5 SAM of intact molecules. EPR spectroscopy provided clear evi-  
dence of the persistence of the radical character of the mole-  
cules upon chemisorption, a result confirmed by state-of-art  
computational approach. The latter allowed to investigate  
10 different absorption scenarios in presence of clean and recon-  
structed surface and evidenced a partial delocalization of the  
radical spin density on the surface. This results in a non-inno-  
cent role of the surface, which is effective in transmitting inter-  
molecular exchange interactions and potentially establish a  
Kondo effect. These interactions are not visible at high  
15 temperature.

Finally, we report the determination of decoherence time  
for nanostructured organic radical, showing that it maintains  
some promise for application in molecular spintronics.  
20

## Conflicts of interest

There are no conflicts to declare.  
25

## Acknowledgements

30 We acknowledge the European COST Action CA15128  
MOLSPIN, the Quanterra ERA-NET Co-fund project SUMO and  
the FET Open Femtotera byte project for financial support.  
Italian MIUR, through PRIN project QCNaMoS (2015-HYFSRT)  
and Progetto Dipartimenti di Eccellenza 2018–2022 (ref. no.  
35 B96C1700020008), and Fondazione Ente Cassa di Risparmio di  
Firenze are also acknowledged for financial support.

## Notes and references

- 1 L. Bogani and W. Wernsdorfer, *Nat. Mater.*, 2008, **7**, 179–186.
- 2 M. Atzori and R. Sessoli, *J. Am. Chem. Soc.*, 2019, **141**, 11339–11352.
- 3 G. Serrano, L. Poggini, M. Briganti, A. L. Sorrentino, G. Cucinotta, L. Malavolti, B. Cortigiani, E. Otero, P. Sainctavit, S. Loth, F. Parenti, A. L. Barra, A. Vindigni, A. Cornia, F. Totti, M. Mannini and R. Sessoli, *Nat. Mater.*, 2020, **19**, 546–551.
- 4 A. Ulman, *Chem. Rev.*, 1996, **96**, 1533–1554.
- 5 D. Gatteschi, R. Sessoli and J. Villain, *Molecular Nanomagnets*, Oxford University Press, 2006.
- 6 V. Lanzilotto, L. Malavolti, S. Ninova, I. Cimatti, L. Poggini, B. Cortigiani, M. Mannini, F. Totti, A. Cornia and R. Sessoli, *Chem. Mater.*, 2016, **28**, 7693–7702.
- 7 G. Fernandez Garcia, A. Lunghi, F. Totti and R. Sessoli, *Nanoscale*, 2018, **10**, 4096–4104.

- 1 8 L. Gragnaniello, F. Paschke, P. Erler, P. Schmitt, N. Barth, S. Simon, H. Brune, S. Rusponi and M. Fonin, *Nano Lett.*, 2017, **17**, 7177–7182.
- 5 9 M. Mannini, L. Sorace, L. Gorini, F. M. Piras, A. Caneschi, A. Magnani, S. Menichetti and D. Gatteschi, *Langmuir*, 2007, **23**, 2389–2397.
- 10 L. Gorini, M. Fabrizioli, M. Mannini, L. Sorace and A. Yakovenko, *Inorg. Chim. Acta*, 2008, **361**, 4089–4093.
- 11 M. Mannini, P. Messina, L. Sorace, L. Gorini, M. Fabrizioli, A. Caneschi, Y. Manassen, P. Sigalotti, P. Pittana and D. Gatteschi, *Inorg. Chim. Acta*, 2007, **360**, 3837–3842.
- 12 M. Mannini, D. Rovai, L. Sorace, A. Perl, B. J. Ravoo, D. N. Reinhoudt, A. Caneschi and B. Jan, *Inorg. Chim. Acta*, 2008, **361**, 3525–3528.
- 15 13 J. L. Gallani, J. Le Moigne, L. Oswald, M. Bernard and P. Turek, *Langmuir*, 2001, **17**, 1104–1109.
- 14 P. Wautelet, J. Le Moigne, V. Videva, P. Turek and J. Le Moigne, *J. Org. Chem.*, 2003, **68**, 8025–8036.
- 20 15 M. Tamura, Y. Nakazawa, D. Shiomi, K. Nozawa, Y. Hosokoshi, M. Ishikawa, M. Takahashi and M. Kinoshita, *Chem. Phys. Lett.*, 1991, **186**, 401–404.
- 16 J. Caro, J. Fraxedas, O. Jürgens, J. Santiso, C. Rovira, J. Veciana and A. Figueras, *Adv. Mater.*, 1998, **10**, 608–610.
- 25 17 R. Kakavandi, S.-A. Savu, A. Caneschi, T. Chassé and M. B. Casu, *Chem. Commun.*, 2013, 10103–10105.
- 18 S. Abb, S.-A. Savu, A. Caneschi, T. Chassé and M. B. Casu, *ACS Appl. Mater. Interfaces*, 2013, **5**, 13006–13011.
- 19 J. Choi, H. Lee, K. Kim, B. Kim and S. Kim, *J. Phys. Chem. Lett.*, 2010, **1**, 505–509.
- 30 20 H. Lee, S. Yang, J. Choi, Y. Park and S. Kim, *J. Phys. Chem. C*, 2011, **115**, 18736–18739.
- 21 A. Robin, L. Marnell, J. Bjork, M. S. Dyer, P. S. Bermudez, S. Haq, S. D. Barrett, M. Persson, A. Minoia, R. Lazzaroni and R. Raval, *J. Phys. Chem. C*, 2009, **113**, 13223–13230.
- 35 22 T. Junghoefer, E. M. Nowik-Boltyk, J. A. De Sousa, E. Giangrisostomi, R. Ovsyannikov, T. Chassé, J. Veciana, M. Mas-Torrent, C. Rovira, N. Crivillers and M. B. Casu, *Chem. Sci.*, 2020, **11**, 9162–9172.
- 40 23 F. Bonosi, G. Gabrielli, G. Martini and M. F. Ottaviani, *Langmuir*, 1989, **5**, 1037–1043.
- 24 J. M. Bennett, O. Warschkow and N. A. Marks, *J. Phys. Chem. C*, 2009, **113**, 1020–1027.
- 45 25 A. Caneschi, F. Ferraro, D. Gatteschi, A. le Lirzin and E. Rentschler, *Inorg. Chim. Acta*, 1995, **235**, 159–164.
- 26 K. Bernot, L. Bogani, A. Caneschi, D. Gatteschi and R. Sessoli, *J. Am. Chem. Soc.*, 2006, **128**(24), 7947–7956.
- 27 L. Bogani, C. Sangregorio, R. Sessoli and D. Gatteschi, *Angew. Chem., Int. Ed.*, 2005, **44**, 5817–5821.
- 50 28 R. Sessoli, M.-E. Boulon, A. Caneschi, M. Mannini, L. Poggini, F. Wilhelm and A. Rogalev, *Nat. Phys.*, 2014, **11**, 69–74.
- 29 A. Collauto, M. Mannini, L. Sorace, A. Barbon, M. Brustolon and D. Gatteschi, *J. Mater. Chem.*, 2012, **22**, 22272.
- 55 30 M. Affronte and F. Troiani, in *Molecular Magnets: Physics and Applications*, ed. J. Bartolomé, F. Luis and J. F. Fernández, Springer, Berlin Heidelberg, 2014, pp. 249–273.
- 31 M. Slota, A. Keerthi, W. K. Myers, E. Tretyakov, M. Baumgarten, A. Ardavan, H. Sadeghi, C. J. Lambert, A. Narita, K. Müllen and L. Bogani, *Nature*, 2018, **561**, 691–695.
- 5 32 F. Ciccullo, A. Calzolari, K. Bader, P. Neugebauer, N. M. Gallagher, A. Rajca, J. Van Slageren and M. B. Casu, *ACS Appl. Mater. Interfaces*, 2019, **11**, 1571–1578.
- 33 H. Atsumi, K. Maekawa, S. Nakazawa, D. Shiomi, K. Sato, M. Kitagawa, T. Takui and K. Nakatani, *Chem. – Eur. J.*, 2012, **18**, 178–183.
- 10 34 L. Poggini, G. Cucinotta, A.-M. M. Pradipto, M. Scarrozza, P. Barone, A. Caneschi, P. Graziosi, M. Calbucci, R. Cecchini, V. A. Dediu, S. Picozzi, M. Mannini and R. Sessoli, *Adv. Mater. Interfaces*, 2016, **3**, 1500855.
- 15 35 R. Frisenda, R. Gaudenzi, C. Franco, M. Mas-Torrent, C. Rovira, J. Veciana, I. Alcon, S. T. Bromley, E. Burzuri and H. S. J. Van Der Zant, *Nano Lett.*, 2015, **15**, 3109–3114.
- 20 36 F. Lombardi, A. Lodi, J. Ma, J. Liu, M. Slota, A. Narita, W. K. Myers, K. Müllen, X. Feng and L. Bogani, *Science*, 2019, **366**, 1107–1110.
- 37 L. Poggini, G. Cucinotta, L. Sorace, A. Caneschi, D. Gatteschi, R. Sessoli and M. Mannini, *Rend. Lincei, Sci. Fis. Nat.*, 2018, **29**, 623–630.
- 25 38 M. H. Dishner, M. M. Ivey, S. Gorer, J. C. Hemminger and F. J. Feher, *J. Vac. Sci. Technol., A*, 1998, **16**, 3295.
- 39 Y. Shirai, L. Cheng, B. Chen and J. M. Tour, *J. Am. Chem. Soc.*, 2006, **128**, 13479–13489.
- 30 40 B. Genorio, T. He, A. Meden and S. Polanc, *Langmuir*, 2008, **24**, 11523–11532.
- 41 J. Vickerman and D. Briggs, *ToF-SIMS: Materials Analysis by Mass Spectrometry*, IM Publications, 2nd edn, 2013.
- 42 C. O'Dwyer, G. Gay, B. Viaris de Lesegno and J. Weiner, *Langmuir*, 2004, **20**, 8172–8182.
- 35 43 D. A. Chernova and A. K. Vorobiev, *J. Polym. Sci., Part B: Polym. Phys.*, 2009, **47**, 107–120.
- 44 S. Stoll and A. Schweiger, *J. Magn. Reson.*, 2003, **163**, 248–256.
- 40 45 A. Bencini, G. Rajaraman, F. Totti and M. Tusa, *Superlattices Microstruct.*, 2009, **46**, 4–9.
- 46 G. Rajaraman, A. Caneschi, D. Gatteschi and F. Totti, *J. Mater. Chem.*, 2010, **20**, 10747–10754.
- 45 47 M. R. Ajayakumar, I. Alcón, S. T. Bromley, J. Veciana, C. Rovira and M. Mas-Torrent, *RSC Adv.*, 2017, **7**, 20076–20083.
- 48 V. Romanov, I. Bagryanskaya, D. Gorbunov, N. Gritsan, E. Zaytseva, D. Luneau and E. Tretyakov, *Crystals*, 2018, **8**, 334.
- 49 Y. Zhang, S. Kahle, T. Herden, C. Stroh, M. Mayor, U. Schlickum, M. Ternes, P. Wahl and K. Kern, *Nat. Commun.*, 2013, **4**, 2110.
- 50 50 G. Rajaraman, A. Caneschi, D. Gatteschi and F. Totti, *Phys. Chem. Chem. Phys.*, 2011, **3**, 3886–3895.
- 51 M. Jaccob, G. Rajaraman and F. Totti, *Theor. Chem. Acc.*, 2012, **131**, 1150.
- 55 52 H. Prüser, P. E. Dargel, M. Bouhassoune, R. G. Ulbrich, T. Pruschke, S. Lounis and M. Wenderoth, *Nat. Commun.*, 2014, **5**, 5417.

1	53 P. G. Barkley, J. P. Hornak and J. H. Freed, <i>J. Chem. Phys.</i> , 1986, <b>84</b> , 1886–1900.	55 V. Lloveras, E. Badetti, J. Veciana and J. Vidal-Gancedo, <i>Nanoscale</i> , 2016, <b>8</b> , 5049–5058.	1
	54 Z. Zhang, A. Berg, H. Levanon, R. W. Fessenden and D. Meisel, <i>J. Am. Chem. Soc.</i> , 2003, <b>125</b> , 7959–7963.	56 V. Chechik, <i>J. Am. Chem. Soc.</i> , 2004, <b>126</b> , 7780–7781.	
5		57 S. S. Eaton and G. R. Eaton, in <i>Biological Magnetic Resonance</i> , 2002, vol. 19, Springer, pp. 29–154.	5
10			10
15			15
20			20
25			25
30			30
35			35
40			40
45			45
50			50
55			55